Santos-Martin, David; Lemon, Scott. (2015). SoL - A PV generation model for grid integration analysis in distribution networks, *Solar Energy*, v. 120, pp.: 549-564.

DOI: https://doi.org/10.1016/j.solener.2015.07.052

SoL – A PV generation model for grid integration analysis in distribution networks

David Santos-Martin *, Scott Lemon

Electric Power Engineering Centre (EPECentre), University of Canterbury, Private Bag 4800, Christchurch 8140, New Zealand

Abstract

Photovoltaic (PV) generation systems are increasingly being integrated into distribution networks, presenting new challenges for network operators and planners. To fully quantify the impact of this distributed generation, power systems and control engineers are often required to model a large number of networks across multiple scenarios of PV uptake and allocation. However, due to the complexity of these network models and simulation methods, and the associated computational constraints, very simplified models are often adopted for solar irradiance, and PV module and inverter output power. These ad hoc models often utilise simple linear relationships, and are not validated against real data or more detailed models. The proposed model (SoL) is composed of pre-existing equations selected from the current state of the art models, as well as newly formulated equations. Each submodel is validated against pre-existing models using data from a number of meteorological sites around the world, showing good performance with reduced computational complexity. The resulting model is subsequently shown to be suitable for running large scale quasi-steady state power flow simulations and Monte Carlo analyses as required for grid integration studies.

Keywords: Distribution network; Irradiance model; Photovoltaic module; Inverter

1. Introduction

Analysing the impact of distributed photovoltaic (PV) generation in low (LV) and medium voltage (MV) distribution networks is computationally complex. Grid integration studies require detailed and accurate models of the network, as well as complete models of load and generation. These models may in turn be used to simulate hundreds or thousands of sites across multiple different network configurations and cases, potentially over large periods of time with resolutions ranging from seconds to hours.

Models for PV generation must encompass the synthesis and processing of irradiance data, the decomposition and transposition of this irradiance onto the plane of the PV array, the conversion of incident irradiance into output power from the PV array and inverter, and the control of the resulting real and reactive AC power. Due to the complexity of these models, and the time required to implement, debug and optimise them, power system engineers and researchers often adopt very simplified ad hoc models of PV generation. These models typically utilise simple linear relationships to describe the output power of the PV system as a function of the irradiance, with minimal validation against existing models. Furthermore, representative PV modules and inverters are often used, without any consideration of the diversity that could be expected

in these elements and their parameters in a real-world network (Thomson and Infield, 2007; Paatero and Lund, 2007; Quezada et al., 2006; Canova et al., 2009; Atwa et al., 2010; Widén et al., 2010).

2. Model description – SoL

The proposed model, referred to as SoL, is composed of nine submodels that fully describe the conversion of irradiance into output power for a representative PV system at any site in a distribution network. Each submodel includes a set of defined input and output variables, and equations which act upon these variables. These equations have been selected from current state of the art models, and in some instances modified or newly formulated, to best fulfil the required trade-offs between accuracy and simplicity of implementation and computational speed. In the trivial case, where no irradiance measurements are available, the output power can be estimated for clear-sky conditions with only three input variables: a vector of time values, the site location, and the inverter rating.

As shown in Fig. 1, the submodels include: the Sun, Solar Geometry, Atmosphere, Array Geometry Design, Horizontal Irradiance, Incident Irradiance, Effective Irradiance, PV Generator – Power Conversion and PV Generator – Power Control. The subsequent sections describe each of these submodels in detail, including the associated variables, the selection or formulation of equations, and the resulting validation.

It should be noted that consistent conventions have been adopted across all models for the definition of temporal and spatial variables. All equations with geographic and spatial variables follow the criteria in ISO 6709 (2008), such that North latitudes and East longitudes are positive. This affects the sign of variables in a number of classical equations in which these values occur. In addition, all azimuth angles or rotational angles in the horizon plane are defined as clockwise from North, such that East is at +90°. Where applicable, the range of valid values and reference basis are also given in the respective table for the model definition.

Any local time values, as expressed using both the hour of the day and the minute of the hour, are referred to the midpoint of the sampling period. For example, if a solar angle is to be computed for an hourly time step, then the first sample should correspond to $t_h = 0$, $t_{min} = 30$ otherwise significant errors may occur due to the offset in time basis.

Finally, all trigonometric equations used in this paper expect arguments to be expressed in degrees.

2.1. Sun

The Sun submodel, presented in Tables 1 and 2, calculates the extraterrestrial irradiance incident on the plane

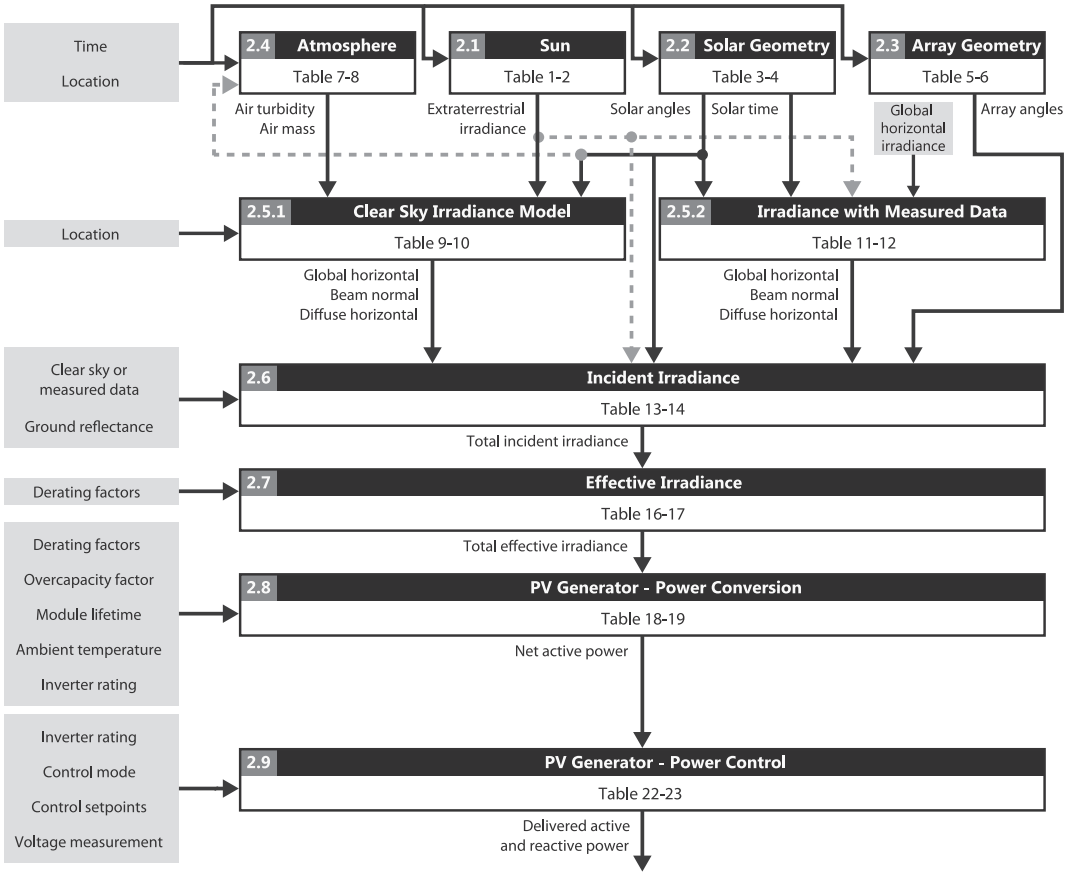

Fig. 1. Flowchart of the SoL model showing submodels and key variables.

Table 1
Sun model variables.

	Variable	Description	Units
Input	n	Day of the year	Integer
Output	H_0	Extraterrestrial irradiance	W m^{-2}

Table 2
Sun model equations.

Id	Equation	References
(1)	$H_0 = 1360.8\left(1 + 0.033\cos\left(360 \cdot \frac{n}{365}\right)\right)$	Duffie and Beckman (1980) pg. 9

normal to the radiation for a given day of the year, n. This model approximates the variation in distance between the Earth and the Sun over a range of ±3.3%.

The equation uses a median value of 1360.8 W m^{-2} for the mean total solar irradiance (TSI), which is commonly referred to as the solar constant. This is the most accurate value of TSI currently available, resulting from measurements by the Total Irradiance Monitor on NASA's Solar Radiation and Climate Experiment (SORCE) and a series of new radiometric laboratory tests by Kopp and Lean (2011). This value is approximately 0.5% lower than the canonical value of 1367.7 W m^{-2} typically used in simple equations for the extraterrestrial irradiance (Duffie and Beckman, 1980).

2.2. Solar Geometry

The Solar Geometry submodel, presented in Tables 3 and 4, describes the solar position in spherical coordinates relative to the local time. The input variables for this submodel are the location of the site, expressed in terms of its latitude and longitude, the local time and its offset from Coordinated Universal Time (UTC), and any offset due to the observance of daylight savings. Vector analysis has recently been used by Sproul (2007) to derive the typical solar geometry equations, and forms the basis for much of the model. The key solar angles relative to the PV system and the local site are shown graphically in Fig. 2.

The set of equations presented in Table 4 assume that the time vector has a resolution on the order of 1 min. If a lower resolution, such as an hourly or daily time step, is desired, then 1 min values should be used for all intermediate calculations before the final results are averaged over the longer time period. While the model can be used for higher temporal resolutions, such as 1–10 s, a loss in accuracy should be expected due to the nature of the approximations made.

The Sun's angular position is defined by the ecliptic longitude, λ, as shown in Eq. (2), which varies from 0° at the March Equinox, to 90° at the June solstice, 180° at the September equinox and 270° at the December solstice, completing 360° after 1 year. Note that the ecliptic period

Table 3
Solar geometry model variables.

	Variable	Description	Range/Units
Input	n	Day of the year	(1–365) d
	t_{hr}	Hour of the day	(0–23) h
	t_{min}	Minute of hour	(0–59) min
	t_{ds}	Daylight savings offset	(−1 or 0) h
	t_{utc}	Difference from UTC time	(−12, +12) h
	ϕ	Site latitude	(−90°, +90°) positive N of equator
	λ_{loc}	Site longitude	(−180°, 180°) positive E of GMT
Output	θ_s	Solar zenith angle	(0°, 90°)
	α_s	Solar altitude angle	(0°, 90°)
	γ_s	Solar azimuth angle	(0°, 360°) clockwise from N
	τ_{sol}	Solar time	widely (−1, 25) h
	δ	Solar declination angle	(−23.44°, 23.44°)
	τ_{eot}	Equation of time	min
	λ_{std}	Standard meridian	(−180°, +180°) positive E of GMT
	ω	Hour angle	widely (−195°, +195°)
	λ	Ecliptic longitude	(−79°, +281°) referred to March Equinox
	ε	Earth obliquity (2000–2050)	23.44°[a]

[a] Default value.

is considered to be 365.25, and no special considerations are needed during leap-years.

The declination of the Sun is simply the angle between the equatorial plane and the line joining the Sun-Earth centres. The selected expression in Eq. (3) uses the current obliquity of the Earth and the ecliptic longitude. While a number of other simple and commonly used expressions exist for the declination, such as $\delta = 23.44\sin\lambda$, the one selected was found to be more accurate with minimal added complexity.

The solar time, as defined by the position of the Sun, differs from the local time as expressed in Eq. (6). This arises due to a number of factors, and is predominantly due to the difference between the location's longitude and the standard merdian against which Coordinated Universal Time (UTC) is referred. The resulting hour angle, ω, shown in Fig. 2, expresses this difference as the solar time referred to solar noon as defined in Eq. (7). For regions which observe daylight savings, a 1 h time variant offset is also required in this expression.

Throughout the year, relative solar time also varies due to the eccentricity of the Earth's orbit and the effect of the Earth's axial tilt. These factors are accounted for in the empirical equation of time. The proposed model was obtained by fitting daily values for the equation of time between the years 2000 and 2050 to the ecliptic longitude. These daily values were calculated using the algorithmic approach described by Meeus (1991), that is used within the Solar Position Algorithm (SPA) by Reda and Andreas (2004). While a number of approximations have

Table 4
Solar geometry model equations.

Id	Equation	References
(2)	$\lambda = \frac{360}{365.25}(n - 81)$	Sproul (2007) pg. 1191
(3)	$\delta = \sin^{-1}(\sin\lambda \sin\varepsilon)$	Sproul (2007) Eq. (16)
(4)	$\tau_{eot} = 9.9\sin(2\lambda) - 7.1\cos\lambda - 1.9\sin\lambda - 0.25\cos(2\lambda)$	Proposed
(5)	$\lambda_{std} = 15 \cdot t_{utc}$	Sproul (2007) pg. 1199
(6)	$\tau_{sol} = (60(t_{hr} + t_{ds}) + t_{min} + 4(\lambda_{loc} - \lambda_{std}) + \tau_{eot})/60$	Sproul (2007) Eq. (30)
(7)	$\omega = 15(\tau_{sol} - 12)$	Sproul (2007) Eq. (7)
(8)	$\theta_s = \cos^{-1}(\sin\phi\sin\delta + \cos\phi\cos\delta\cos\omega)$	Sproul (2007) Eq. (18)
(9)	$\alpha_s = 90 - \theta_s$	Duffie and Beckman (1980) pg.13
(10)	$\gamma_s = \begin{cases} \gamma_c, & \text{if } \omega < 0 \\ 360 - \gamma_c, & \text{otherwise} \end{cases}$ where $\gamma_c = \cos^{-1}\left(\frac{\sin\delta\cos\phi - \cos\delta\sin\phi\cos\omega}{\cos\alpha_s}\right)$	Sproul (2007) Eq. (23) Szokolay (2007) pg.35

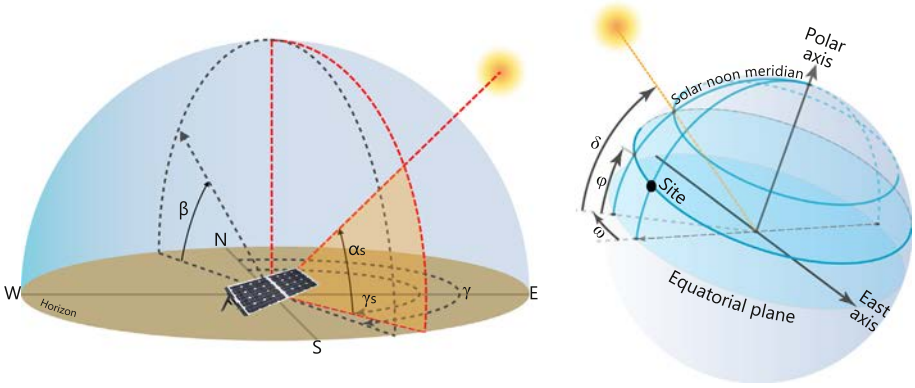

Fig. 2. PV module and site angles, and solar geometry angles. Adapted from Brownson (2013).

been formulated for the equation of time, the one proposed in Eq. (4) has been found to be more accurate than similar expressions described by Spencer (1971), Lamm (1981) and Reno et al. (2012) for the time period of analysis, with an RMSE of 17 s and a maximum error less than 45 s.

The solar angles relative to the site, altitude and azimuth, use the horizon plane as a reference and are expressed in spherical coordinates as shown graphically in Fig. 2. The solar zenith angle, which is the complement of the solar altitude, can be derived using vector analysis as presented in Eq. (8).

The solar azimuth is the angle in the horizon plane between the projection of the vector linking the Earth-Sun centres and the North Pole axis. This angle is defined as 0° to the north, and increasing clockwise such that east is +90°. While a number of simple trigonometric equations can be found for the solar azimuth in the literature, the one selected in Eq. (10) avoids further expressions or conditionals for resolving the correct quadrant.

2.3. Array Geometry design

The Array Geometry submodel, presented in Tables 5 and 6, describes the proposed criteria for selecting the optimum PV array tilt and azimuth angles for a given location.

Table 5
Array geometry design variables.

	Variable	Description	Range/Units
Input	ϕ	Site latitude	(−90°, +90°) positive N of equator
	λ_{loc}	Site longitude	(0°, 360°) positive E of GMT
output	β	Tilt of the PV array from horizontal	(0°, 90°)
	γ	Azimuth angle of the PV from North	(0°, 360°)

Table 6
Array geometry design equations.

Id	Equation	References
(11)	$\gamma = \begin{cases} 180 \text{ if } \phi \in (0, 90), & \text{Northern hemisphere} \\ 0 \text{ if } \phi \in (-90, 0), & \text{Southern hemisphere} \end{cases}$	Proposed
(12)	$\beta = -0.004\phi^2 + a\cdot \mid \phi \mid + b$ where $\begin{cases} a = 1.13, b = 0 & \text{if clear} - \text{sky irradiance} \\ a = 0.92, b = 2 & \text{if measured weather irradiance} \end{cases}$	Proposed

This is done in a similar manner to other studies such as that by Yadav and Chandel (2013), but in this instance using global data. Note that this orientation corresponds to that orientation which maximises the total annual energy generated by the PV system. Alternative tilt and azimuth angles may be used in place of those calculated using the proposed model so as to maximise energy generated over alternative periods of time, as defined by site specific requirements.

To formulate these design equations, more than 2500 locations were selected across the world, as shown in Fig. 4. These correspond to those locations for which typical meteorological year (TMY) data is publicly available from the EnergyPlus database (U.S. Department of Energy, 2015). For each of these locations, the PV array orientation yielding the maximum annual energy over a year was calculated using both typical meteorological year and clear sky irradiance data.

The incident irradiance was calculated for every PV array configuration with a tilt between 0° and 90°, and an azimuth between −90° and 90° in steps of 1°. To estimate the incident irradiance from the global horizontal, direct normal and diffuse horizontal irradiance a transposition algorithm based on that by Perez et al. (1992) was used. This transposition process is explained in more detail in Section 2.6. The resulting incident irradiance was summed over a year, and the orientation that yielded the maximum annual energy was selected.

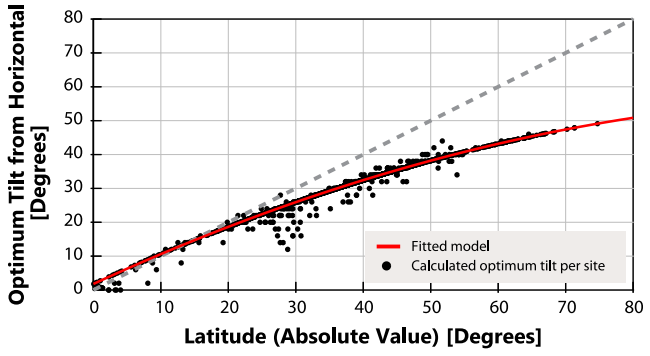

Fig. 3. Fitted model for the optimum PV system tilt angle as a function of the system latitude, using real irradiance data.

The optimum tilt was fitted against the absolute value of the latitude for all sites using least-squares, as shown in Fig. 3. The resulting equation, as in Eq. (12), had an acceptable goodness of fit value of $R^2 = 0.982$. In addition, annual energy calculated using the proposed model was found to deviate from that computed using the true optimum by less than 0.5% for approximately 95% of the sites.

A similar process was performed for the same sites using modelled clear sky data. The global horizontal, direct normal and diffuse horizontal clear sky values were calculated using the approach by Perez et al. (2002). A common rule of thumb for selecting the tilt of a PV system, under clear sky conditions, is to set it equal to the latitude. While this is suitable for lower latitudes, with a deviation in annual energy from the optimum within 0.1%, it yields suboptimal configurations for latitudes further than 50° from the equator. Beyond 70° the annual energy deviation from the true optimum is greater than 2% using this rule. As such, an additional model has been fitted for clear sky conditions, as in Eq. (12). This yields configurations with an annual energy deviation less than 0.1% from the optimum for any latitude, with a goodness of fit of $R^2 = 0.99$.

The optimum azimuth angle of a PV array varies based on the variability of incident irradiance within a day across the year. For example, repeated periods of morning fog or evening storms will result in the optimum azimuth shifting to the east or west so as to account for the reduced irradiance during those times. However, due to the stochastic nature of this variability across locations, no simple rule exists for the optimum azimuth of a PV panel under real conditions at any location. As such, the model uses the theoretical optimum azimuth, whereby PV arrays in the Southern hemisphere are oriented due north (0°), and arrays in the Northern hemisphere due south (180°) as in Eq. (11). This is a common practice for most real-world installations. A sensitivity analysis for all of the sites found that the difference in the maximum daily irradiance value for all azimuth angles between ±20° from the proposed criteria was bounded within ±5% at a 90% confidence level.

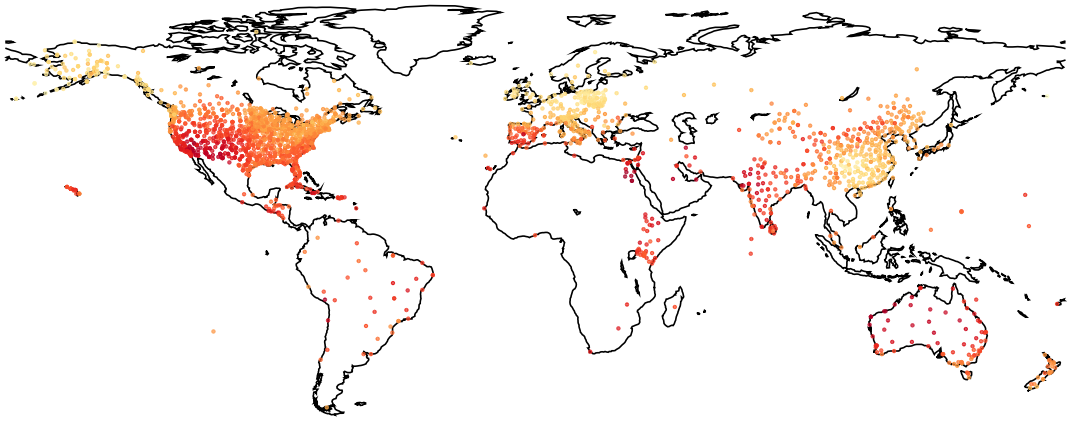

Fig. 4. World map of meteorological sites used for model validation.

Table 7
Atmosphere variables.

	Variable	Description	Range/Units
input	n	Day of the year	(1–365) d
	ϕ	Site latitude	(−90°, +90°) positive N of equator
	h	Site elevation	m
input[a]	α_s	Solar altitude angle	(0°, 90°)
output	T_L	Linke turdity factor	pu
	AM	Absolute air mass	pu
	p	Air pressure	Pa
	AM_0	Relative air mass	pu

[a] Input from another submodel.

2.4. Atmosphere

The atmosphere submodel, presented in Tables 7 and 8, describes the factors leading to the attenuation of extraterrestrial irradiance through the atmosphere, such as air molecules, aerosols and water vapour.

To calculate the irradiance at ground level from the extraterrestrial irradiance, the path length of the radiation through the atmosphere must be considered. This path length is described using the air mass coefficient, which is defined as the ratio of the mass of the atmosphere through which beam radiation passes to the mass it would pass through if the sun were at its zenith. An air mass of 0 (AM0) corresponds to extraterrestrial conditions in the absence of an atmosphere, while an air mass of 1 (AM1) corresponds to the path when the sun is directly overhead. The air mass factor may be defined with respect to sea level or to a specific elevation or distance above sea level, which are referred to as the relative and absolute air mass respectively.

The model selected to calculate the relative air mass, as in Eq. (14), is an empirical relationship by Kasten and Young (1989) that is valid for zenith angles approaching 90°. The correction factor to assess the absolute air mass described in Eq. (15) uses the pressure defined in Eq. (13) as a function of the site elevation.

The extraterrestrial irradiance is also attenuated due to absorption and scattering by aerosols, which is referred to as atmospheric turbidity. The Linke turbidity factor, as first described by Linke (1922), is a very convenient approximation to model this attenuation. It describes the optical thickness of the atmosphere due to water vapour and aerosol particles, effectively measuring the number of clean atmospheres that would be necessary to produce the same attenuation of the extraterrestrial solar radiation as the real atmosphere. Typical values range from 2 for very clean, cold air to 8 for heavily polluted air (Eltbaakh et al., 2012).

Global maps of Linke turbidity, with a normalized air mass value of 2 (AM2), have been computed for each month of the year by Remund et al. (2003) using a combination of ground measurements and satellite data. These are made publicly available by Remund et al. (2012). These maps have been used to compute a piecewise model of Linke turbidity across a year for different zones, as in Eq. (16).

The data was first processed to select only those Linke turbidity values above land, as shown in Fig. 5. For each of the five geographic zones in Eq. (16), the median Linke turbidity value was computed for each month. A sinusoidal model was subsequently fitted to describe the daily variability of Linke turbidity across a year. The goodness of fit ranges from $R^2 = 0.85$ with a root-mean-square error of 0.17 over the year, to $R^2 = 0.99$ and a root-mean-square error of 0.05 depending on the zone.

Note, that for each 1 unit increase in the Linke turbidity factor, the peak daily clear sky irradiance will decrease by a factor on the order of 5%. In instances where the atmosphere above the site is heavily polluted, the Linke turbidity factor must be increased. Some authors such as Bason (2004), Eltbaakh et al. (2012), and Calinoiu et al. (2013), suggest a value of 7–8 for these sites.

2.5. Horizontal irradiance models

To accurately quantify the impact of distributed PV within a distribution network, real world irradiance data should ideally be used. This data is commonly obtained using local meteorological stations, synthesised using statistical models, or estimated using satellite imagery. In

Table 8
Atmosphere equations.

Id	Equation	Refs
(13)	$p = 100\left(\frac{44331.514-h}{11880.516}\right)^{1/0.1902632}$	PSAS (2004) Eq. (9)
(14)	$AM_0 = \frac{1}{\left(\sin\alpha_s + 0.50572(6.07995+\alpha_s)^{-1.6364}\right)}$	Kasten and Young (1989) Eq. (3)
(15)	$AM = AM_0\,\frac{p}{101325}$	Gueymard (1993) pg. 125
(16)	$T_L = a + b\cos(\omega \cdot n)$	Proposed
	where $\begin{cases} a=1.8, b=0 & \text{if } \lvert\phi\rvert > 60°, \text{Poles} \\ a=3.8, b=0.56, \omega=1.13 & \text{if } -23.44° > \phi > 0°, \text{South tropic} \\ a=4.25, b=-0.46, \omega=0.94 & \text{if } 23.44° > \phi > 0°, \text{North tropic} \\ a=3, b=-0.84, \omega=0.94 & \text{if } 60° \geqslant \phi \geqslant 23.44°, \text{North zone} \\ a=3.2, b=0.36, \omega=0.94 & \text{if } -60° \leqslant \phi \leqslant -23.44°, \text{South zone} \end{cases}$	

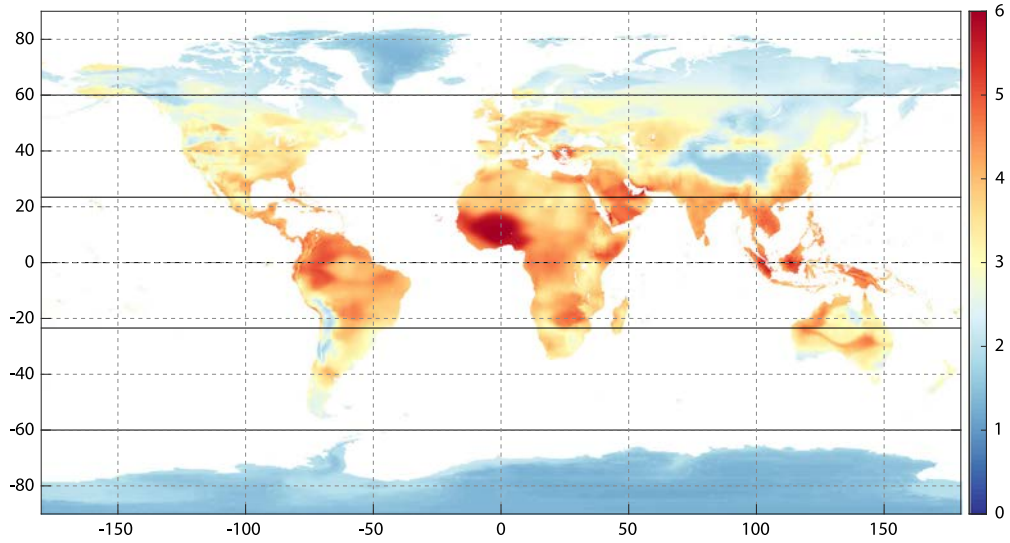

Fig. 5. World map of the mean annual Linke tubidity factor.

Table 9
Clear sky model variables.

	Variable	Description	Range/ Units
Input	h	Site elevation	m
input[a]	H_0	Extraterrestrial radiation	W m^{-2}
	θ_s	Solar zenith angle	(0°, 90°)
	AM	Absolute air mass	pu
	T_L	Linke turdity factor	pu
Output	$G_{h,c}$	Global horizontal irradiance	W m^{-2}
	$G_{bn,c}$	Beam (direct) normal irradiance	W m^{-2}
	$G_{dh,c}$	Diffuse horizontal irradiance	W m^{-2}
	f_{h1}, f_{h2}, c_{g1}, c_{g2}	Factors	pu

[a] Input from another submodel.

some studies, pyranometers are installed specifically for the purpose of gathering suitable horizontal or in-plane incident irradiance data (Thomson and Infield, 2007). In instances where no measured data is available, or only an approximate or worst-case analysis is desired, then clear sky models can be used to describe the irradiance at any time in the absence of clouds.

The two models presented in this section describe the calculation of clear sky global horizontal, direct normal and diffuse horizontal irradiance, as well as the decomposition of measured global horizontal irradiance into direct normal and diffuse horizontal components. All the irradiance variables in the following subsections, will use variables and subscript symbols according to Beckman et al. (2002), where the subscript (h) corresponds to horizontal, (n) to normal, (i) to incident, (c) to clear sky and (m) to measured real weather data.

2.5.1. Clear sky irradiance model

A number of approaches have been developed to calculate the clear sky irradiance at a site given the extraterrestrial irradiance. These range from simple models which only account for attenuation due to solar geometry and air mass, to more complex equations which model additional atmospheric quantities, such as air pressure, temperature, relative humidity, aerosol content and Rayleigh scattering (Reno et al., 2012).

The selected model, presented in Tables 9 and 10, has been shown by Reno et al. (2012) to have significantly higher accuracy than comparable models, without requiring site specific measurements. This model, as described by Perez et al. (2002) and Ineichen and Perez (2002), uses the extraterrestrial irradiance and the solar position as inputs, and then incorporates the effect of the atmosphere

Table 10
Clear sky model equations.

Id	Equation	References
(17)	$f_{h1} = \exp(-h/8000), f_{h2} = \exp(-h/1250)$	Ineichen and Perez (2002) eq. nomenclature
(18)	$c_{g1} = 0.0000509 \cdot h + 0.868, c_{g2} = 0.0000392 \cdot h + 0.0387$	Perez et al. (2002) pg.311
(19)	$G_{h,c} = H_0 \cos\theta_s c_{g1} \cdot \exp\{-c_{g2} AM \cdot [f_{h1} + f_{h2}(T_L - 1)]\} \cdot \exp(0.01 AM^{1.8})$	Perez et al. (2002) pg. 311
(20)	$G_{bn,c} = \min\left\{H_0\left(0.664 + \frac{0.163}{f_{h1}}\right)\exp(-0.09AM \cdot (T_L - 1)), \frac{G_{h,c}}{\cos\theta_s}\left(1 - \frac{0.1 - 0.2\cdot\exp\{-T_L)\}}{0.1 + 0.882/f_{h1})}\right)\right\}$	Perez et al. (2002) pg.312
(21)	$G_{dh,c} = G_{h,c} - G_{bn,c}\cos\theta_s$	Brownson (2013) pg.214

characteristics and site elevation using a set of empirical expressions as shown in Eqs. (19)-(21). Note, that this model is consistent with the Linke turbidity values at AM2 obtained previously.

2.5.2. Irradiance with measured data

In instances when measured global horizontal irradiance is available, a decomposition model is still required to estimate the direct normal and diffuse horizontal components. These are in turn required to transpose the irradiance onto the desired plane of the PV array. Decomposition models are typically based on the correlation between the clearness index and the diffuse fraction. The clearness index is defined as the ratio of the global horizontal irradiance to the extraterrestrial horizontal irradiance, while the diffuse fraction is the ratio of the diffuse to global horizontal irradiance (Boland et al., 2013).

According to Torres et al. (2010) and Bertrand et al. (2015), the most accurate ground-based models are the BRL model described by Ridley et al. (2010) and Lauret et al. (2013), and the DIRINT model described by Perez et al. (1992). Although all models present limitations when the global irradiance is dominated by the diffuse portion, or when smaller sub-hourly time periods must be considered, the final result remains acceptable for the purposes of the developed model Bertrand et al. (2015).

Table 11
Measured data model (BRL) variables.

	Variable	Description	Range/Units
Input	$G_{h,m}$	Global horizontal irradiance	W m^{-2}
input[a]	H_0	Extraterrestrial irradiance	W m^{-2}
	τ_{sol}	Solar time	widely $(-1, 25)$ h
	θ_s	Solar zenith angle	(0°, 90°)
output	$G_{dh,m}$	Diffuse horizontal irradiance	W m^{-2}
	$G_{bn,m}$	Beam (direct) normal irradiance	W m^{-2}
	k_T	Clearness index over the sampling period	pu
	K_{Td}	Daily clearness index	pu
	ψ_t	Persistent factor	pu
	k_d	Diffuse fraction factor	pu

[a] Input from another submodel.

The BRL model, as presented in Tables 11 and 12, has been selected due to its accuracy and simplicity. It is based on a multiple predictor diffuse fraction model as shown in Eq. (25), using the hourly clearness index, daily clearness index, solar time, solar elevation as well as a persistence factor, ψ_t, described in Eq. (24). The persistence factor is used to account for the inertia of the sky conditions by means of the lag and lead of the clearness index, shifted by one sample. This expression is only valid for times between sunrise and sunset, and is set equal to the subsequent or preceding value of the clearness index at each of the endpoints respectively.

Note that the clearness index, as expressed in Eq. (22), is the ratio of the instantaneous global horizontal irradiance and the extraterrestrial irradiance projected on the horizontal surface at the midpoint of the sampling period. To avoid singular values the clearness index is only computed for solar altitude angles higher than 5°. The daily clearness index Eq. (23) is computed in a similar manner, but using average values to perform the ratio.

2.6. Incident irradiance

To compute the irradiance on the plane of a PV array (POA) for a given tilt and azimuth, it is necessary to calculate the incident beam, sky diffuse, and ground reflected components. While the beam component can be computed from a simple geometric relationship with the direct normal irradiance, the other two diffuse components must be estimated from isotropic or anisotropic models, and empirical correlations (Duffie and Beckman, 1980; Brownson, 2013). The selected model for calculating the total incident irradiance is shown in Tables 13 and 14. The irradiance variables used as inputs in this section may originate from either the clear sky or measured weather data models, and thus no subscripts are used when referring to them.

The beam component contribution to the incident irradiance is obtained using Eq. (29) via a simple projection from the beam normal irradiance into the normal of the desired surface, with an incident angle obtained from Eq. (28).

The diffuse irradiance reflected from the ground into the plane of the array is assumed to be isotropic, originating

Table 12
Measured data model (BRL) equations.

Id	Equation	References
(22)	$k_T = \begin{cases} 0, & \text{if } \theta_s > 85° \\ \frac{G_{h,m}}{(H_0 \cos\theta_s)}, & \text{otherwise} \end{cases}$	Duffie and Beckman (1980) Eq. (2.9.3)
(23)	$K_{Td} = \frac{\sum_{day} G_{h,m}}{\sum_{day} H_0 \cos\theta_s}$	Duffie and Beckman (1980) Eq. (2.9.2)
(24)	$\psi_t = (k_{t-1} + k_{t+1})/2$	Ridley et al. (2010) Eq. (6)
(25)	$k_d = \frac{1}{1+\exp(-5.323+7.279\,k_T-0.03\,\tau_{sol}-0.005\,\alpha_s+1.719\,K_{Td}+1.082\,\psi_t)}$	Lauret et al. (2013) Eq. (9)
(26)	$G_{dh,m} = G_{h,m} \cdot k_d$	Boland et al. (2013) Eq. (7)
(27)	$G_{bn,m} = \frac{G_{h,m}-G_{dh,m}}{\cos\theta_s}$	Boland et al. (2013) Eq. (7)

uniformly from the ground with a view factor from the ground to the array of $(1-cos\beta)/2$, as shown in Eq. (30). The reflectance of the ground is referred to as the albedo, and has a value between 0 and 1. While the albedo value is important in accurately determining the incident irradiance, no reliable database of values has been found. Models typically assume a default value of 0.2 across sites, based on the work by Liu and Jordan (1963). In snowy conditions, a higher albedo value closer to 0.7 is more suitable. If this change in albedo is ignored, then errors in the peak daily power as high as 10% may be observed when using the default value.

The remaining incident component is the contribution from the diffuse sky irradiance. A large number of models have been developed that attempt to correlate the diffuse irradiance on a tilted surface to that measured on a horizontal surface such as those by Liu and Jordan (1963), Hay and Davies (1980) and by Perez et al. (1990). Significant research has also been devoted to assessing the performance of these models under different conditions for different locations, such as by Reindl et al. (1990a), Loutzenhiser et al. (2007), Evseev and Kudish (2009), and by Gueymard (2009). The simplest of these models, namely that of Liu and Jordan (1963), considers the incident diffuse irradiance to be isotropic, with the received solar radiation originating uniformly across the entire sky dome. Other anisotropic models, such as those analysed by Loutzenhiser et al. (2007), add more subcomponents like circumsolar and horizon brightness.

For selecting the most suitable model, seven models have been assessed and their accuracy compared to the model described by Perez et al. (1990), which is computationally intensive but has been shown to have good accuracy. These models include the isotropic model (I) by Liu and Jordan (1963), the Willmott model (W) by Willmott (1982), the Skartveit-Olseth (SO) model by Skartveit and Olseth (1986), the Hay-Davies (HD) model by Hay and Davies (1980), the Reindl model (R) by Reindl et al. (1990b) and Reindl et al. (1990a), the Klucher model (K) by Klucher (1979), and the Muneer model (M) by Muneer (1997).

From Figs. 6 and 7 it can be seen that all of the models fall within an RMSE of approximately 60 W m^{-2} and typically tend to underestimate the diffuse incident irradiance across all sites. In general, as additional subcomponents and correction factors are added to the anisotropic model, its accuracy increases for the majority of sites. However, this comes at the cost of increased implementation complexity and decreased speed, as shown in Table 15. The computational speed of each model was calculated by dividing the computation time of the Perez model by the total computation time of the respective model and averaging across all trials. The Hay-Davies model was deemed to achieve the best trade-off between computational complexity and accuracy of those models examined, with a similar RMSE to the more complicated Reindl, Klucher and Muneer models, and an average computation time approximately 7 times as fast as the Perez model. It was thus selected for use in the final model as in Eq. (33).

2.7. Effective irradiance

The effective irradiance on the plane of the PV array is given by the incident irradiance less any losses due to shading or panel soiling as described in Tables 16 and 17.

The shading factor ultimately depends on the environment of the location under analysis. As the model is primarily intended for use in analyses where the values of interest, such as overvoltage, are mainly related to high irradiance values, this factor can typically be neglected. In most cases it is thus assumed that at times of high irradiance the solar altitude angle is sufficiently high so as to

Table 13
Incident irradiance variables.

	Variable	Description	Range/Units
Input	ρ_g	Ground reflectance factor (albedo)	0.2[a] pu
Input [b]	G_h ($G_{h,m}$ or $G_{h,c}$)	Global horizontal irradiance	W m^{-2}
	G_{bn}($G_{bn,m}$ or $G_{bn,c}$)	Beam (direct) normal irradiance	W m^{-2}
	G_{dh}($G_{dh,m}$ or $G_{dh,c}$)	Diffuse horizontal irradiance	W m^{-2}
	γ_s	Solar azimuth angle	(0°, 360°) clockwise from N
	α_s	Solar altitude angle	(0°, 90°)
	β	Tilt of the PV array from horizontal	(0°, 90°)
	γ	Azimuth angle of the PV array from North	(0°, 360°)
	H_0	Extraterrestrial irradiance	W m^{-2}
output	G_i	Total incident irradiance	W m^{-2}
	Θ	Angle of incidence	(0°, 90°)
	G_{bi}	Beam (direct) incident irradiance	W m^{-2}
	G_{ri}	Reflected incident irradiance	W m^{-2}
	G_{di}	Diffuse incident irradiance	W m^{-2}
	A	Anisotropic index	pu
	R_b	Geometric factor for beam irradiance	pu

[a] Default value.
[b] Input from another submodel.

Table 14
Incident irradiance equations (for Clear Sky Model or Measured Irradiance Data).

Id	Equation	References
(28)	$\Theta = \cos^{-1}\left(\sin\beta\cos\alpha_s\cos\left(\gamma-\gamma_s\right)+cos\beta\sin\alpha_s\right)$	Sproul (2007) Eq. (28)
(29)	$G_{\mathrm{bi}} = G_{\mathrm{bn}}\cdot\cos\Theta$	Sproul (2007) Eq. (25)
(30)	$G_{\mathrm{ri}} = \rho_g\frac{(1-\cos\Theta)}{2}\cdot G_{\mathrm{h}}$	Liu and Jordan (1963) Eq. (11), Loutzenhiser et al. (2007) Eq. (3)
(31)	$A = \frac{G_{\mathrm{bn}}}{H_0}$	Hay and Davies (1980)
(32)	$R_b = \frac{\cos\Theta}{\cos(90-\alpha_s)}$	Hay and Davies (1980)
(33)	$G_{\mathrm{di}} = G_{\mathrm{dh}}\left(AR_b+(1-A)\left(\frac{1+cos\beta}{2}\right)\right)$	Hay and Davies (1980)
(34)	$G_{\mathrm{i}} = G_{\mathrm{bi}}+G_{\mathrm{di}}+G_{\mathrm{ri}}$	Liu and Jordan (1963) Eq. (11)

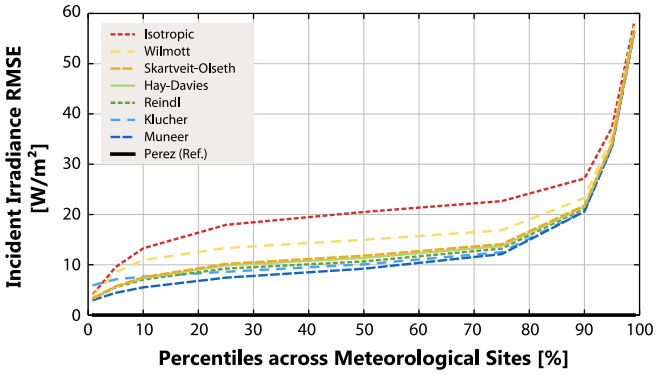

Fig. 6. Root-mean-square error across meteorological sites for each diffuse model relative to the Perez model.

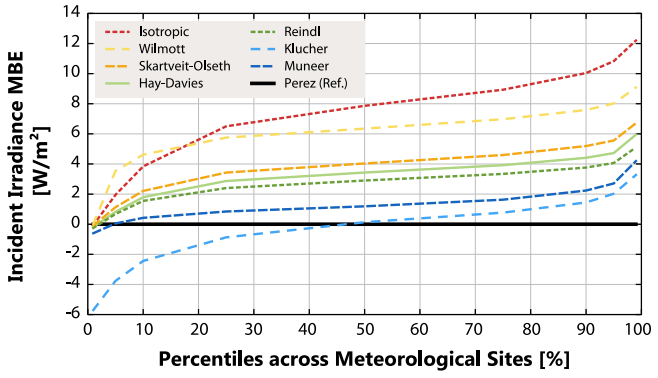

Fig. 7. Mean bias error across meteorological sites for each diffuse model relative to the Perez model.

limit shading from nearby buildings. By default, the shading derate factor is set to 1, although a value closer to 0.97 should be used if the model is used to assess generated energy as suggested by Duffie and Beckman (1980) and Dobos (2014).

The effective irradiance available for conversion into electrical energy is also reduced due to soiling, such as dust accumulation on panels. By default a soiling derating factor of 0.98 is used, as suggested by Duffie and Beckman (1980) and Dobos (2014). However, depending on the latitude and consequent tilt of the PV panels, and local

Table 15
Median computational speed and RMSE of diffuse irradiance models relative to the Perez model across all sites.

Median values	Model						
	I	W	SO	HD	R	K	M
Speed	62.1	9.8	5.5	6.8	3.8	3.6	2.6
RMSE [W m^{-2}]	20.5	15.0	11.8	11.4	10.7	10.0	9.2

Table 16
Effective irradiance variables.

	Variable	Description	Range/Unit
Input	η_s	Soiling derate factor	0.98[a] pu
	η_{sh}	Shading derate factor	1[a] pu
Input[b]	G_{i}	Total incident irradiance	W m^{-2}
Output	E	Total effective irradiance	W m^{-2}

[a] Default value.
[b] Input from another submodel.

Table 17
Effective irradiance equations.

Id	Equation	References
(35)	$E = G_{\mathrm{i}}\eta_s\eta_{sh}$	Dobos (2014) Table 6

weather conditions, this may vary significantly between sites. For example, Mani and Pillai (2010) and Qasem et al. (2014) found that for more arid areas, the PV module power output could be reduced by 10–30% due to dust build up if periodic cleaning was not carried out.

2.8. PV Generator – power conversion

The goal of this section is to obtain a simple model that expresses the PV system power as a function of meteorological variables, such as irradiance and temperature, as well as characterising the performance of real modules and inverters. The resulting power conversion related equations are presented in Tables 18 and 19.

The method to obtain the proposed PV power conversion model is divided into four steps: normalise variables; define an array design; compute a regression model; and obtain the net output power considering derating factors.

Table 18
PV Generator variables – power conversion.

	Variable	Description	Range/Units
Input	S_{stc}	Inverter rating at STC conditions	VA
	η_m	Mismatch derate factor	0.98[a] pu
	η_w	Wiring derate factor	0.98[a] pu
	η_c	Connections derate factor	0.995[a] pu
	η_{lo}	Initial light induced degradation factor	0.985[a] pu
	η_{np}	Nameplate derate factor	0.99[a] pu
	t_{age}	Lifetime of the PV modules	(0–30) years
	R_{oc}	Overcapacity factor	1.05[a] pu
	T_{amb}	Ambient temperature	20[a] °C
Input [b]	E	Total effective irradiance	W m^{-2}
Output	P_n	Net active power	W
	E_{pu}	Normalised total effective irradiance	pu
	ΔT	Temperature difference	°C
	$E_{pu,a}$	Normalised total effective irradiance in the array	pu
	η_l	Light induced degradation factor	0.985[a] pu

[a] Default value.
[b] Input from another submodel.

Table 19
PV generator equations – power conversion.

Id	Equation	References
(36)	$E_{pu} = E/800$	Proposed
(37)	$\Delta T = T_{amb} - 20$	Proposed
(38)	$E_{pu,a} = \frac{R_{oc}}{1.05} E_{pu}$	Proposed
(39)	$P_g = S_{stc} \cdot [0.846 E_{pu,a} - 0.106 E_{pu,a}^2 - 0.00368 E_{pu,a} \Delta T]$	Proposed
(40)	$\eta_l = \eta_{lo} - 0.005 t_{age}$	Jordan and Kurtz (2013) pg.21
(41)	$P_n = P_g \cdot \eta_m \eta_w \eta_c \eta_l \eta_{np}$	Proposed

2.8.1. Normalisation process

There are three relevant variables that directly affect the performance of the PV modules and their subsequent output power: the total effective irradiance, the ambient temperature and the wind speed. In this model only the first two are considered, with the impact of wind speed treated as negligible and thus set to a fixed value of 1 m s^{-1} for simplification purposes. Both variables are normalised against NOCT reference values of irradiance and temperature in Eqs. (36) and (37) for the purposes of regression modelling.

2.8.2. PV array design

The total power rating of the PV array is given by the product of the rating of the selected PV module and the number of units in the array. It is common practice by designers and installers to size the PV inverter based on the rated power of the PV array. They may either approximately match the inverter rating to the total installed PV array rating, or undersize it by some factor to compensate for module degradation over time or to optimize economic returns. A common criteria used is to size the inverter to between 70% and 80% of the rated power of the array (Chen et al., 2013; Demoulias, 2010). In the model fitting step, the PV array is sized such that it contains the minimum number of modules to just exceed the inverter rating, while also fulfilling its operating voltage constraints. Across all the PV module and inverter combinations this criteria resulted in the PV array rating either being exactly matched to the inverter rating or being sized slightly larger, with a median overcapacity factor of 1.05. This value is subsequently used as the default overcapacity factor.

2.8.3. Regression modelling

A number of empirical regression models have been developed in the literature, which relate the PV system output power or performance to the pertinent meteorological parameters (Kimber et al., 2009; ASTM, 2013; Skoplaki and Palyvos, 2009). These approaches typically use multiple linear regression methods to calculate the coefficients relating irradiance, temperature and, in some instances wind speed, to the system output power using real measurements.

The proposed approach is to synthetically reproduce these measurements using common empirical models for the PV modules and inverters, simulating all possible module-inverter combinations. To ensure that a representative selection of current generation PV systems are modelled, two public databases with detailed information for commercial PV modules and inverters have been used. To simulate the PV modules the five-parameter single-diode equivalent model described by Soto et al. (2006) is used, with module data from the California Energy Com-

mission (California Energy Commission, 2015). The module temperature is calculated using the Sandia array performance model (King et al., 2004). To simulate the inverters, the empirical Sandia inverter model as described by King et al. (2007) is used, with inverter data from NREL (2014).

The total number of components considered, after disregarding those with invalid information, is 10,018 mono- and polycrystalline PV modules and 537 inverters with ratings between 1 and 30 kW. A brief summary of the data used from these databases is shown in Table 20, which shows that the median PV module and inverter rating in the dataset correspond to 234 W and 4 kW respectively.

The total number of all module-inverter combinations is on the order of 5×10^6, which presents particular challenges for simulation and fitting. For all of these possible combinations with the described PV array design process, the median overcapacity factor is 1.05. Subsequently, the normalised total effective irradiance on the array can be defined as in Eq. (38).

The regression model is completed using the synthetic data given by each of the mentioned combinations simulated at irradiance values ranging from 0 to 1200 W m^{-1} in 10 W m^{-2} steps; and ambient temperature values from −10 to +40 °C in 5 °C steps.

The resulting model shown in (Eq. (39)) has a goodness-of-fit $R^2 = 0.994$. The summary of the error as a function of the irradiance and ambient temperature is presented in Table 21. In this table it is shown that the error percentiles are bounded within ±7% for most of the module-inverter combinations across all irradiance and temperature values.

Table 20
Statistics of PV modules and inverters from databases.

	Percentiles						
	1	5	25	50	75	95	99
Inverters (kW)	1.5	1.7	3.0	4.0	6.0	11.4	20.0
Modules (W)	60	135	200	234	260	310	405

Table 21
PV Generator model error (%) as a function of irradiance and temperature.

Temp. °C	Irradiance W m^{-2}	Percentiles				
		1	5	50	95	99
0	250	−3.2	−2.4	−0.7	1.5	2.5
	500	−4.0	−3.0	0.0	4.2	6.0
	1000	−6.3	−4.7	0.3	1.6	1.6
10	250	−3.1	−2.4	−0.7	1.4	2.3
	500	−3.9	−2.9	−0.1	3.9	5.7
	1000	−6.1	−4.6	0.3	6.2	6.2
20	250	−3.2	−2.5	−0.8	1.2	2.1
	500	−4.0	−3.0	−0.2	3.7	5.3
	1000	−6.2	−4.6	0.2	7.2	10.3
30	250	−3.3	−2.6	−0.9	1.0	1.9
	500	−4.1	−3.1	−0.3	3.4	5.0
	1000	−6.6	−4.7	0.1	6.8	9.9

2.8.4. Derating factors

In addition to the shading and soiling effects, which reduce the effective irradiance received by the modules, there are other derating factors that affect the net output power of the PV system. The most relevant are shown in Table 18, and include losses due to wiring and connections, and mismatch between modules. The proposed default values for these factors are as described by Dobos (2014).

As PV modules are exposed to light their performance is also expected to degrade over time, which is encapsulated by the light induced degradation factor in Eq. (40). Based on an analytical review of photovoltaic degradation rates by Jordan and Kurtz (2013), a median yearly degradation value of 0.5%/year for silicon-based modules is used. Finally, in Eq. (41) all of the derating factors are applied to the gross power to obtain the net output power of the system.

2.9. PV generator – power control and protection

With the accelerating uptake of distributed PV, and the consequent impacts on network voltage, inverters are increasingly being required to implement grid support functionality. As such, it is now common for inverters to be configured in a range of operating modes such that they adjust their active or reactive power output as a function of voltage or power (IEC, 2013) to assist in maintaining the voltage within operational limits. An additional power control and protection submodel has thus been included, as described in Tables 22 and 23, to model this functionality.

The fixed power factor mode, shown in Eq. (42), allows the inverter to operate at a constant power factor, typically 0.8–0.95 leading/laging. Note, that small inverters typically derate the active power when providing any reactive power to respect the rated apparent power and prevent the thermal capabilities of the inverter being exceeded. This is done by activating the overload protection function and operating the inverter in a suboptimal mode.

The Volt-Var mode controls the inverter to absorb or inject reactive power depending on the voltage levels so as to support the network when needed. A typical application of this function is shown in Fig. 8, with the algorithm described in Eq. (43). Note that the effect of this mode on the voltage will highly depend on the network properties, such as the R/X ratio.

The Volt-Watt mode linearly reduces the active power delivered by the inverter as the voltage level increases before reaching the threshold for disconnection, as described in Eq. (44). Note, that this function may significantly impact the profitability of the generation plant if the active power is consistently being curtailed. In addition, when the PV system is connected within a radial network, the location along the feeder will affect the extent of this curtailment. Systems that are connected towards the end of the feeder will be required to reduce their active power

Table 22
PV generator variables – power control.

	Variable	Description	Range/Units
Input	Mode	Inverter control mode	Fixed PF, Volt-Watt, Volt-Var, PF-Watt
	PF	Inverter displacement power factor	(0–1)
	V	Measured average voltage supplied by the grid	V
	S_{stc}	Inverter rating at STC conditions	VA
	V_1, V_2, V_3, V_4	Voltage thresholds to define control characteristics	V
Input[a]	P_n	net active power	W
Output	P	Delivered active power	W
Output	Q	Delivered reactive power	VAr
	K_{derate}	Derate limit for active power with Mode = Volt-Watt	0.2[b] pu
	Q_{lead}, Q_{lag}	Reactive power limits with Mode = Volt-Var	VAr
	PF_{max}	Power factor limit with Mode = PF-Watt	(0–1)

[a] Input from another submodel.
[b] Default value.

Table 23
PV generator equations – power control.

Id	Equation	References
(42)	Mode = Fixedpowerfactor :	IEC (2013) pg. 39
	$P = \begin{cases} P_n & \text{if } P_n < S_{stc} \cdot PF \\ S_{stc} \cdot PF & \text{otherwise} \end{cases}$	
	$Q = P\sqrt{\frac{1-PF^2}{PF^2}}$	
(43)	Mode = Volt − Var	IEC (2013) Fig. 14
	$P = \begin{cases} P_n & \text{if } Q^2 + P_n^2 < S_{stc}^2 \\ \sqrt{(S_{stc}^2 - Q^2)} & \text{otherwise} \end{cases}$	
	$Q = \begin{cases} Q_{lead} & \text{if} V \leqslant V_1 \\ Q_{lead}\left(\frac{V_2-V}{V_2-V_1}\right) & \text{if } V_1 < V < V_2 \\ 0 & \text{if } V_2 \leqslant V \leqslant V_3 \\ Q_{lag}\left(\frac{V-V_3}{V_4-V_3}\right) & \text{if } V_3 < V < V_4 \\ Q_{lag} & \text{if } V \geqslant V_4 \end{cases}$	
(44)	Mode = Volt − Watt	IEC (2013) Fig. 32
	$P = \begin{cases} P_n & \text{if } V \leqslant V_3 \\ P_n\left(1 - (V - V_3)\frac{1-K_{derate}}{V_4-V_3}\right) & \text{if } V_3 < V < V_4 \\ K_{derate} \cdot P_n & \text{if } V \geqslant V_4 \end{cases}$	
	$Q = 0$	
(45)	Mode = PF − Watt	IEC (2013) Fig. 31
	$P = P_n$	
	$Q = P\sqrt{\frac{1-PF^2}{PF^2}}$	
	$PF = \begin{cases} 1 & \text{if } \frac{P}{S_{stc}} \leqslant 0.5 \\ 1 - \left(\frac{P}{S_{stc}} - 0.5\right)\frac{1-PF_{max}}{0.5} & 0.5 < \frac{P}{S_{stc}} \leqslant 1 \end{cases}$	

to a greater extent, due to the higher impedance from the head of the feeder and consequently higher voltage rise.

The Watt-Power Factor mode controls the operating power factor of the inverter depending on the generated active power, as described in Eq. (45).

Finally, the inverter should disconnect from the grid and cease any power exchange if the magnitude of the grid voltage remains outside the defined operation range for a sustained period of time. In the model this threshold voltage is considered an average value, typically over a period of 10 min.

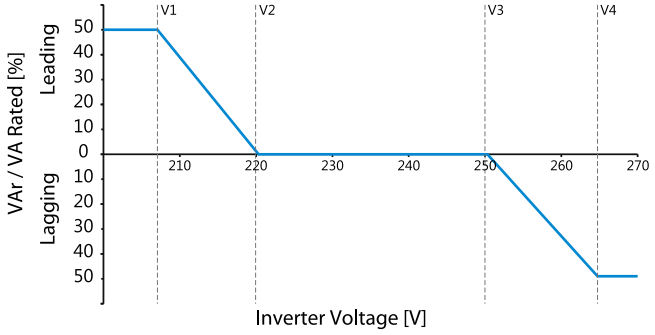

Fig. 8. Generic Volt-Var control mode characteristic, showing configurable voltage set-points.

3. Model validation

The SoL model has been validated against a selection of well-established, more detailed models using both synthesised clear sky irradiance and real-world irradiance data. For each of these cases, the output power is computed for 100 PV systems at each of the 2500 sites previously described. The empirical CDFs of module and inverter ratings from the CEC module database and Sandia inverter database are uniformly sampled, and 100 modules and inverters randomly selected with the corresponding ratings.

For the full clear sky case, the atmospheric airmass and Linke turbidity models have been implemented according to Muhammad (1983) and Remund et al. (2012). The global horizontal, direct normal and diffuse horizontal irradiance values have been calculated using the approach by Ineichen and Perez (2002). Alternatively, for the real-world irradiance case the same set of locations as previously described and shown in Fig. 4 are used, with typical meteorological year values for the irradiance components, temperature and wind speed.

Table 24
Percentiles of percentage error (full – SoL) for the clear sky case by world regions.

Zone	Percentiles				
	5	25	50	75	95
North	−4.6	−0.4	0.0	0.0	4.0
South	−2.0	0.0	0.0	0.9	5.5
Tropics	−2.6	0.0	0.0	0.4	4.7

Table 25
Percentiles of percentage error (full – SoL) for the real weather data case by world regions.

Zone	Percentiles				
	5	25	50	75	95
North	−2.5	0.0	0.0	0.0	5.3
South	−4.9	0.0	0.0	0.0	6.4
Tropics	−2.5	0.0	0.0	0.0	4.5

In both cases, for the full comparison model the extraterrestrial irradiance has been calculated as described by Duffie and Beckman (1980); the solar angles are calculated using the Solar Position Algorithm (SPA) described by Reda and Andreas (2004); the incident irradiance is calculated using the diffuse sky model by Perez et al. (2002). To simulate the output power of each of the PV systems, the same set of models described in the regression modelling step is used, with the efficiency factors described by Dobos (2014).

The percentage error between the output power for the full model and the SoL model is calculated at each point in time for each PV system at each location. The percentiles across time for all systems in each geographic region were subsequently calculated, as shown in Tables 24 and 25 for the clear sky and real-data cases respectively. The SoL model shows lower errors for clear sky data, particularly for regions outside the tropics. For both cases the error is bounded within ±6.4% at any location, across all times and for any system within a 90% confidence level. Furthermore, on average, the SoL model exhibited a computational speed on the order of 5–10 times that of the full model, averaged across all 250,000 validation cases.

4. Conclusions

A simplified model, SoL, has been developed for the fast calculation of the output power of a representative PV system for use in grid integration studies by power systems engineers. It may be used to calculate the maximum output of a typical PV system at a given location under clear-sky conditions, or to produce more realistic output time series given real meteorological data such as global horizontal irradiance and temperature.

The model is comprised of pre-existing and newly formulated equations, which have been deemed to meet the necessary trade-off between accuracy, ease of implementation, and computational complexity. The newly proposed equations include criteria for estimating the optimum orientation of a PV system given its location, a piecewise Linke turbidity model, and a representative PV system representing the average performance of more than 5×10^6 real module-inverter combinations, considering only mono-and polycrystalline PV modules.

The SoL model has been validated using hourly typical meteorological year data at over 2500 sites worldwide, exhibiting a relatively low error within ±6.4% for most system combinations and sites compared to more detailed and sophisticated models. This error is likely to increase if it is used for system configurations that differ from those proposed, such as modelling the performance of alternative technologies like thin film modules, or for modelling different array configurations in which tracking is utilised or for which mutual shading of modules must be considered.

Acknowledgment

The authors would like to acknowledge the funding provided by theMinistry of Business Innovation and Employment, Transpower, and the EEA for the GREEN Grid project.

References

ASTM, 2013. Standard test method for reporting photovoltaic non-concentrator system performance. http://dx.doi.org/10.1520/e2848.

Atwa, Y., El-Saadany, E., Salama, M., Seethapathy, R., 2010. Optimal renewable resources mix for distribution system energy loss minimization. Power Syst., IEEE Trans. 25 (1), 360–370.

Bason, F., 2004. Diffuse solar irradiance and atmospheric turbidity. In: Euro Sun 2004 Conference Proceedings, Freiburg, Germany. pp. 1–7.

Beckman, W., Bugler, J., Cooper, P., Duffie, J., Dunkle, R., Glaser, P., Horigome, T., Howe, E., Lawand, T., van der Mersch, P., Page, J., Sheridan, N., Szokolay, S., Ward, G., 2002. Units and symbols in solar energy. Solar Energy 72 (1), III–V, http://www.sciencedirect.com/science/article/pii/S0038092X01001049.

Bertrand, C., Vanderveken, G., Journée, M., 2015. Evaluation of decomposition models of various complexity to estimate the direct solar irradiance over Belgium. Renew. Energy 74, 618–626.

Boland, J., Huang, J., Ridley, B., 2013. Decomposing global solar radiation into its direct and diffuse components. Renew. Sustain. Energy Rev. 28, 749–756.

Brownson, J.R., 2013. Solar Energy Conversion Systems. Academic Press.

California Energy Commission, 2015. CEC PV Calculator Version 5.0. Tech. rep., California Energy Commission, USA. <http://gosolarcalifornia.org/tools/nshpcalculator/download_calculator.php>.

Calinoiu, D., Paulescu, M., Ionel, I., Stefu, N., Pop, N., Boata, R., Pacurar, A., Gravila, P., Paulescu, E., Trif-Tordai, G., 2013. Influence of aerosols pollution on the amount of collectable solar energy. Energy Convers. Manage. 70, 76–82.

Canova, A., Giaccone, L., Spertino, F., Tartaglia, M., 2009. Electrical impact of photovoltaic plant in distributed network. Ind. Appl., IEEE Trans. 45 (1), 341–347.

Chen, S., Li, P., Brady, D., Lehman, B., 2013. Determining the optimum grid-connected photovoltaic inverter size. Solar Energy 87, 96–116.

Demoulias, C., 2010. A new simple analytical method for calculating the optimum inverter size in grid-connected {PV} plants. Electric Power

Syst. Res. 80 (10), 1197–1204, http://www.sciencedirect.com/science/article/pii/S0378779610000866.
Dobos, A.P., 2014. PVWatts Version 5 Manual. Tech. rep., National Renewable Energy Laboratory (NREL), Golden, CO.
Duffie, J.A., Beckman, W.A., 1980. Solar Engineering of Thermal Processes. Wiley, New York.
Eltbaakh, Y.A., Ruslan, M., Alghoul, M., Othman, M., Sopian, K., Razykov, T., 2012. Solar attenuation by aerosols: an overview. Renew. Sustain. Energy Rev. 16 (6), 4264–4276.
Evseev, E.G., Kudish, A.I., 2009. The assessment of different models to predict the global solar radiation on a surface tilted to the south. Solar Energy 83 (3), 377–388.
Gueymard, C., 1993. Critical analysis and performance assessment of clear sky solar irradiance models using theoretical and measured data. Solar Energy 51 (2), 121–138.
Gueymard, C.A., 2009. Direct and indirect uncertainties in the prediction of tilted irradiance for solar engineering applications. Solar Energy 83 (3), 432–444.
Hay, J.E., Davies, J.A., 1980. Calculation of the solar radiation incident on an inclined surface. In: Proc. of First Canadian Solar Radiation Data Workshop, Ministry of Supply and Services Canada. Vol. 59. pp. 59–72.
IEC, 2013. 61850-90-7 TR – Communication networks and systems for power utility automation-Part 90-7: IEC 61850 object models for power converters in distributed energy resources (DER) systems.
Ineichen, P., Perez, R., 2002. A new airmass independent formulation for the Linke turbidity coefficient. Solar Energy 73 (3), 151–157.
ISO 6709, 7 2008. Iso 6709:2008 – standard representation of geographic point location by coordinates. Tech. rep., International Organization for Standardization.
Jordan, D.C., Kurtz, S.R., 2013. Photovoltaic degradation rates – an analytical review. Progress Photovolt.: Res. Appl. 21 (1), 12–29.
Kasten, F., Young, A.T., 1989. Revised optical air mass tables and approximation formula. Appl. Opt. 28 (28), 4735–4738.
Kimber, A., Dierauf, T., Mitchell, L., Whitaker, C., Townsend, T., Newmiller, J., King, D., Granata, J., Emery, K., Osterwald, C., Myers, D., Marion, B., Pligavko, A., Panchula, A., Levitsky, T., Forbess, J., Talmud, F., June 2009. Improved test method to verify the power rating of a photovoltaic (PV) project. In: Photovoltaic Specialists Conference (PVSC), 2009 34th IEEE. pp. 000316–000321.
King, D., Boyson, W., Kratochvill, J., 2004. Photovoltaic array performance model. Tech. Rep. SAND2004-3535, Sandia National Laboratories, USA. <http://prod.sandia.gov/techlib/access-control.cgi/2004/043535.pdf>.
King, D.L., Gonzalez, S., Galbraith, G.M., Boyson, W.E., 2007. Performance model for grid-connected photovoltaic inverters. Tech. Rep. SAND2007-5036, Sandia National Laboratories, USA. <http://energy.sandia.gov/wp/wp-content/gallery/uploads/Performance-Model-for-Grid-Connected-Photovoltaic-Inverters1.pdf>.
Klucher, T.M., 1979. Evaluation of models to predict insolation on tilted surfaces. Solar Energy 23 (2), 111–114.
Kopp, G., Lean, J.L., 2011. A new, lower value of total solar irradiance: evidence and climate significance. Geophys. Res. Lett. 38 (1).
Lamm, L., 1981. A new analytic expression for the equation of time. Solar Energy 26 (5), 465.
Lauret, P., Boland, J., Ridley, B., 2013. Bayesian statistical analysis applied to solar radiation modelling. Renew. Energy 49, 124–127.
Linke, F., 1922. Transmissions-koeffizient und Trübungsfaktor. Beitr. Phys. Fr. Atmos 10, 91–103.
Liu, B.Y., Jordan, R.C., 1963. The long-term average performance of flat-plate solar-energy collectors: with design data for the US, its outlying possessions and Canada. Solar Energy 7 (2), 53–74.
Loutzenhiser, P., Manz, H., Felsmann, C., Strachan, P., Frank, T., Maxwell, G., 2007. Empirical validation of models to compute solar irradiance on inclined surfaces for building energy simulation. Solar Energy 81 (2), 254–267.
Mani, M., Pillai, R., 2010. Impact of dust on solar photovoltaic (pv) performance: research status, challenges and recommendations. Renew. Sustain. Energy Rev. 14 (9), 3124–3131.
Meeus, J.H., 1991. Astronomical Algorithms. Willmann-Bell, Incorporated..
Muhammad, I., 1983. An Introduction to Solar Radiation. Academic, Vancouver.
Muneer, T., 1997. Solar Radiation and Daylight Models for the Energy Efficient Design of Buildings. Architectural Press, Oxford.
NREL, 2014. SAM 2014.1.14 photovoltaic and wind component libraries. Tech. rep., National Renewable Energy Laboratory, USA. <https://sam.nrel.gov/content/component-databases>.
Paatero, J.V., Lund, P.D., 2007. Effects of large-scale photovoltaic power integration on electricity distribution networks. Renew. Energy 32 (2), 216–234.
Perez, R., Ineichen, P., Moore, K., Kmiecik, M., Chain, C., George, R., Vignola, F., 2002. A new operational model for satellite-derived irradiances: description and validation. Solar Energy 73 (5), 307–317.
Perez, R., Ineichen, P., Seal, R., Maxwell, E., Zalenka, A., 1992. Dynamic global-to-direct irradiance conversion models. ASHRAE Trans. 98 (1), 354–369.
Perez, R., Ineichen, P., Seals, R., Michalsky, J., Stewart, R., 1990. Modeling daylight availability and irradiance components from direct and global irradiance. Solar Energy 44 (5), 271–289.
PSAS, 2004. A quick derivation relating altitude to air pressure. Tech. rep., Portland State Aerospace Society, USA. <http://psas.pdx.edu/RocketScience/PressureAltitude_Derived.pdf>.
Qasem, H., Betts, T.R., Müllejans, H., AlBusairi, H., Gottschalg, R., 2014. Dust-induced shading on photovoltaic modules. Progress Photovolt.: Res. Appl. 22 (2), 218–226.
Quezada, V.M., Abbad, J.R., Roman, T.G.S., 2006. Assessment of energy distribution losses for increasing penetration of distributed generation. Power Syst., IEEE Trans. 21 (2), 533–540.
Reda, I., Andreas, A., 2004. Solar position algorithm for solar radiation applications. Solar Energy 76 (5), 577–589.
Reindl, D., Beckman, W., Duffie, J., 1990a. Evaluation of hourly tilted surface radiation models. Solar Energy 45 (1), 9–17.
Reindl, D.T., Beckman, W.A., Duffie, J.A., 1990b. Diffuse fraction correlations. Solar Energy 45 (1), 1–7.
Remund, J., Wald, L., Lefevre, M., Ranchin, T., Page, J., 2003. Worldwide Linke turbidity information. In: ISES Solar World Congress 2003. Vol. 400. International Solar Energy Society (ISES), pp. 13–p.
Remund, J., Wald, L., Lefevre, M., Ranchin, T., Page, J., 2012. SODA Solar Radiation Data. Tech. rep., SODA Solar Radiation Data, France. <http://www.soda-is.com/eng/services/climat_free_eng.php#c5>.
Reno, M.J., Hansen, C.W., Stein, J.S., 2012. Global horizontal irradiance clear sky models: Implementation and analysis. SANDIA report SAND2012-2389.
Ridley, B., Boland, J., Lauret, P., 2010. Modelling of diffuse solar fraction with multiple predictors. Renew. Energy 35 (2), 478–483.
Skartveit, A., Olseth, J.A., 1986. Modelling slope irradiance at high latitudes. Solar Energy 36 (4), 333–344.
Skoplaki, E., Palyvos, J., 2009. On the temperature dependence of photovoltaic module electrical performance: a review of efficiency/power correlations. Solar Energy 83 (5), 614–624.
Soto, W.D., Klein, S., Beckman, W., 2006. Improvement and validation of a model for photovoltaic array performance. Solar Energy 80 (1), 78–88, http://www.sciencedirect.com/science/article/pii/S0038092X05002410.
Spencer, J., 1971. Fourier series representation of the position of the sun. Search 2 (5), 172-172.
Sproul, A.B., 2007. Derivation of the solar geometric relationships using vector analysis. Renew. Energy 32 (7), 1187–1205.
Szokolay, S.V., 2007. Solar geometry. PLEA: Passive Low Energy Arch. Int.
Thomson, M., Infield, D., 2007. Impact of widespread photovoltaics generation on distribution systems. Renew. Power Gener., IET 1 (1), 33–40.

Torres, J., De Blas, M., García, A., De Francisco, A., 2010. Comparative study of various models in estimating hourly diffuse solar irradiance. Renew. Energy 35 (6), 1325–1332.

U.S. Department of Energy, 2015. Weather data. <http://apps1.eere.energy.gov/buildings/energyplus/weatherdata_about.cfm>.

Widén, J., Wäckelgård, E., Paatero, J., Lund, P., 2010. Impacts of distributed photovoltaics on network voltages: stochastic simulations of three Swedish low-voltage distribution grids. Electric Power Syst. Res. 80 (12), 1562–1571.

Willmott, C.J., 1982. On the climatic optimization of the tilt and azimuth of flat–plate solar collectors. Solar Energy 28 (3), 205–216.

Yadav, A.K., Chandel, S., 2013. Tilt angle optimization to maximize incident solar radiation: a review. Renew. Sustain. Energy Rev. 23, 503–513.